

Phase equilibria in an athermal solution of platelike particles

Dagmara Sokolowska and Jozef K. Moscicki*

Smoluchowski Institute of Physics, Jagiellonian University, Reymonta 4, 30-059 Krakow, Poland

(Received 18 August 1999; revised manuscript received 11 February 2000)

A molecular frame lattice theory of athermal solutions of platelike particles is presented. Steric repulsion between the particles is assumed to be the sole interaction present in the system (the athermal limit). The theory is developed for flat rectangular parallelepipeds, and examined in detail for two opposite shape anisotropy limits: rods and square boards. Numerical calculations show that in a pure system of either long rods or square boards, a nematic phase is formed once the shape anisotropy exceeds some critical value: for rods the critical aspect ratio x_r^{crit} is 8.019, and for boards x_d^{crit} is 3.742. For higher values of the ratio, a narrow concentration region of coexistence for the nematic and isotropic phases, which separates the isotropic (low concentration) from the nematic (high concentration) solution, is found on dilution of each system.

PACS number(s): 64.70.Md, 61.30.Cz

I. INTRODUCTION

In discussing the fundamental molecular properties of a system forming a nematic phase, the importance of two opposite kinds of interactions, steric repulsion and specific attractions, is usually emphasized and treated [1–4]. Among the variety of molecular theories of the nematic state stressing the dominance of one or the other kind of forces, Flory championed the steric point of view with the aid of a lattice method [5]. In his very first attempt to use the lattice to simplify the specification of spatial configurations, and to evaluate the steric factor in the configuration partition function, the relevant partition function was factorized into the configuration or steric part Z_{comb} , the orientational part Z_{or} , and a part Z_{int} accounting for the exchange free energies of interaction between molecules of the system, $Z = Z_{\text{comb}}Z_{\text{or}}Z_{\text{int}}$ [2]. Use of the cubic lattice associated with the laboratory reference frame (XYZ lattice) of the sample is pivotal for the method. Each rodlike molecule becomes segmented into a sequence of contiguous rodlike subsegments positioned in adjacent rows parallel to the nematic director $\hat{\mathbf{n}}$. In equilibrium, the statistics of subsegments in the rows should be the same and independent of each other. Steric constraints for rods in three dimensions are thus transformed into a one dimensional problem of randomly distributed solvent molecules with polydispersity in the length subsegments, where the polydispersity function is defined by the equilibrium orientational distribution function of the rods. However, the need to map molecules onto subsegments on the lattice limits the number of orientations available to the rod to a discrete spectrum of orientations only.

The original lattice theory of Flory has been explored over the years to study different aspects of rodlike systems [4–7]. A significant improvement to the lattice idea is due to Warner [8,9]. Without losing the original advantages of placing a system of rods on the lattice, Warner proposed a clever alternative lattice approach that allowed him to remove discretization of the orientational states of a rod. He noted that what determines the mapping of molecular configurations

onto the lattice representation is the projection y of the molecule onto the plane perpendicular to the director [2]. Thus, alternatively, the lattice can be associated with the reference frame of the rod (xyz lattice) and the rest of the system projected onto the plane perpendicular to the long axis of the given rod. The discretization imposed on the rod orientation by the XYZ lattice is thus removed. Orientational disorder of the system is measured by the mean projection of the rods, called after Warner the *steric constraint* \bar{p} . The critical value of the rod aspect ratio x for the formation of a stable nematic phase in a pure, athermal system of rodlike molecules is predicted by Warner's method to be somewhat higher than that obtained with the Flory method [10–12]. However, because of it, Warner's latent entropy at the transition is smaller than the one predicted from the XYZ lattice, which overestimates the latent entropy.

It has been demonstrated recently that XYZ lattice methods are also suitable for application to discotic molecules, cf., e.g., [13–15]. For this purpose, a much more severe simplification of the disk molecular shape is required, namely, the disk is approximated by a flat, rectangular parallelepiped, in order to fit the lattice. Wnek and Moscicki [14,15], in their extension of the Flory model for rods [2] to the case of discotics, considered the formation of a uniaxial nematic phase by square parallelepipeds. For symmetry reasons, the representation of perfectly ordered discotics on the XYZ lattice by square boards of aspect ratio x and thickness equal to the lattice unit cell in this particular case is rather well justified [14]. In the spirit of the Flory method, disorientation of the disks was introduced into the system by two independent rotations of each board (or, simply, disk) about the X and Y laboratory frame axes. This procedure transforms disks into stairways, in which the stairway steps form trains of contiguous segments located in neighboring elementary XY slices of the lattice. For the same reasons as for rods, the situation in each XY slice is statistically identical at equilibrium, and the three dimensional problem is transformed into the problem of accommodating different trains in a two dimensional sea of other trains and solvent molecules. The model allowed a study of the system in the presence of solute-solvent interactions [14,15] and a system of discotic molecules with sidechains [15]. The minimum (critical) value of the disk

*Electronic address: ufmoscic@cyf-kr.edu.pl

anisotropy sufficient for formation of a stable nematic phase calculated from the theory is $x^{\text{crit}}=3.015$ [14]. Despite reasonable success, such a treatment of the hard disk system is only approximate. Disk orientations in space are severely discretized, particles are not allowed to rotate freely about the symmetry axis, and the axis has a discrete spectrum of orientations. Consequently, accounting for the solute-solute attractive intermolecular interactions usually present in liquid crystals is beyond the scope of the calculations in [14].

In order to remove some limitations of [14] and address thermotropic nematics, and, in particular, to extend our quest to the contemporary and very attractive problem of biaxial nematics, we have developed an approach for a system of plate- or boardlike [16] particles along Warner's idea of using the molecular frame lattice xyz . In particular, the use of the xyz lattice accommodates the preservation of plate rigidity and complete orientational freedom. It makes the modeling of interactions of any kind, i.e., steric repulsion as well as attractive forces between particles, feasible, natural, and easy to handle. The theory converges to proper results in the perfect order limit of a pure system of both rods and square boards (for simplicity, hereafter referred to as disks), where the entropy per lattice site approaches zero [17,18]. Moreover, in order to maintain the thermodynamic correctness of the model, the ideal mixing term in the Gibbs free energy [19], arising from the presence of solute and solvent particles in the system, is naturally incorporated in the formalism. The role of the plate biaxiality and of soft dispersion interactions between plates will be addressed elsewhere [20].

The paper is organized as follows. The aim of the next section is to present a general outline of the lattice treatment of steric interactions in an athermal solution of platelike particles, i.e., the only interaction accounted for is contact repulsion, and the configurational partition function is evaluated. Results of the calculations specialized to rods and to disks are presented and discussed in the light of results available in the literature in the final section of the paper.

II. THEORY

A. The anisotropic phase

The results of the lattice method in describing phase equilibria in rodlike systems [5,6,8] are the substrate upon which much of our work on systems of disklike [14,15] and plate-like molecules is based. The theory presented here concerns the phase transitions and phase equilibria in a system of identical platelike particles dispersed in a solvent. The ultimate goal is to find the partition function Z relevant to the problem. Once Z is known, and thus the Gibbs function of the ensemble, G , one can study the equilibrium properties of the system. To attain equilibrium of the anisotropic phase it is required that the equilibrium orientational distribution of plates minimizes the free energy. In order to handle the problem we introduce three reference frames, the laboratory reference frame $\{XYZ\}$ whose Z axis is assumed to be parallel to the direction of orientational order, and two molecular reference frames. The first $\{xyz\}$, is associated with the test plate. The second, $\{xyz^k\}$, is of a randomly selected plate, the k th, say. Each molecular frame is defined in such a way that its z axis is along the plate normal $\hat{\mathbf{n}}$. We employ $\Omega^i \equiv (\alpha^i, \beta^i, \gamma^i)$ to indicate the orientation of one reference

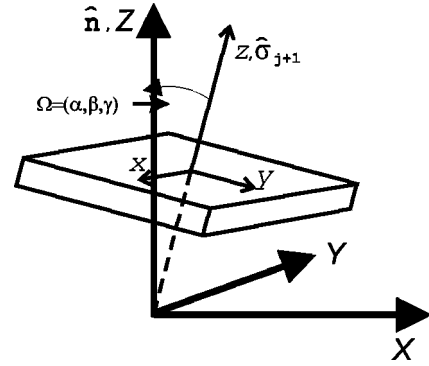


FIG. 1. Orientation of the molecular reference frame of the test plate $\{xyz\}$ with respect to the laboratory reference frame $\{XYZ\}$.

frame with respect to another; cf. the scheme in Eq. (1) and Fig. 1, as a set of three Euler angles [21]. The Euler angles are chosen in such a way as to bring the initial frame into coincidence with the final frame, so that the first angle α^i defines a rotation about the z axis of the initial frame:

$$\begin{aligned} \Omega & \\ \{XYZ\} & \rightarrow \{xyz\}, \\ \Omega' & \\ \{XYZ\} & \rightarrow \{xyz^k\}, \\ \Omega^k & \\ \{xyz\} & \rightarrow \{xyz^k\}. \end{aligned} \quad (1)$$

The equilibrium orientation distribution ensures that

$$\left. \frac{\partial G}{\partial n_\Omega} \right|_{\text{eq}} = \left. \frac{\partial(-k_B T \ln Z)}{\partial n_\Omega} \right|_{\text{eq}} = 0 \quad (2)$$

over all angles, where n_Ω is the number of plates whose orientation is Ω . Similarly, the equilibrium coexistence of the isotropic (I) and anisotropic (A) phases imposes the condition that the chemical potentials of the solvent μ_s and solute μ_x (obtained as partial derivatives of the free energy) in the two phases must be equal at equilibrium, i.e.,

$$\left. \frac{\mu_i^I}{k_B T} = \frac{\mu_i^A}{k_B T} \right|_{\text{eq}}, \quad i = s, x. \quad (3)$$

In calculating the partition function, the present theory follows the general framework of earlier work from our group [14,15]. What is significantly different is that in calculating the steric factor Z_{comb} we introduce an auxiliary lattice not in the reference frame of the system, but in the molecular frame of the plate under consideration (the test plate). To facilitate comparison between past and present lattice work on discotic molecules, we try to use the same notation as before [8,14].

The solute under consideration consists of n_x monodisperse plates with principal aspect ratios x_1 and x_2 . We choose the unit cell of the molecular reference lattice to have linear dimension of the plate thickness, so that a plate on the lattice is represented by a rectangular parallelepiped of dimensions x_1 by x_2 . For simplicity and convenience, the solvent molecules are assumed to be isodiametric, with diam-

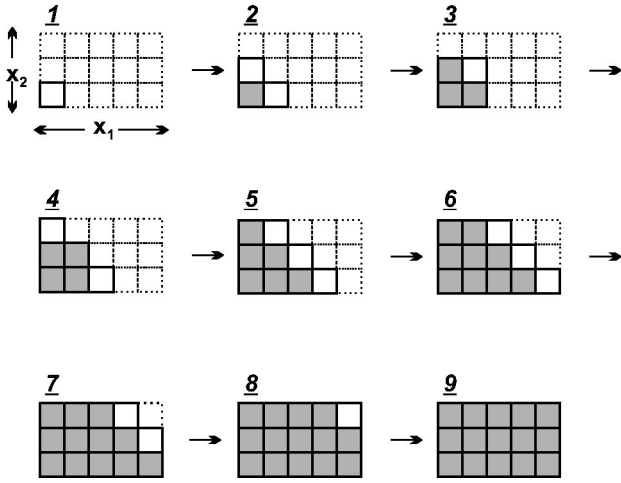


FIG. 2. Sequence of placing of test particle elementary cells on the lattice.

eter equal to the plate thickness. Hence, the solvent aspect ratio is $x_s = 1$. All particles of the ensemble are incapable of interpenetrating each other (steric constraint), and no voids are allowed in the system [22]. Therefore, the total number of lattice cells necessary to accommodate our system, i.e., the system volume in unit cell units, is

$$n_0 = n_s + x_1 x_2 n_x. \quad (4)$$

In a standard initial step of the lattice method, we assume that j plates have already been assigned locations in the system volume. To evaluate the configuration part of the partition function, Z_{comb} , we calculate the expected number of locations ν_{j+1} accessible to an additional (test) $(j+1)$ th plate. The auxiliary reference lattice is associated with $\{xyz\}$ in such a way that the x and y axes are along the x_1 and x_2 side edges of the test plate, respectively.

We make the usual assumption that in equilibrium all locations accessible to the test plate are statistically equivalent. This translates in the lattice approach into stipulating that in equilibrium all elementary slices of the lattice parallel to each other are statistically equivalent, i.e., we assume that in any given slice dispersion of the contributions from all plates of the system and of the solvent molecules is random, being uninfluenced by the configuration of neighboring slices. Furthermore, the thermodynamic properties of the system should not depend on the order of filling the sample volume with plates.

In contrast to the $\{XYZ\}$ lattice in the Flory method, our test molecule when inserted into the elementary xy slice of its own lattice is not segmented and remains intact. This alone constitutes a substantial simplification of our calculations.

We apply the following sequential algorithm for placing elementary cells of the $(j+1)$ th molecule on the lattice; cf. Fig. 2. We begin by anchoring the plate by placing one of its corner cells 2. Second, we position two edge cells adjacent to the anchor cell 3. These are followed by the adjacent interior cell 4 and the next two edge cells 5. This establishes the construction boundary more or less perpendicular to the plate diagonal. We advance the construction boundary row

by row until completion of the task; cf. 6–9 in Fig. 2. The final result should depend neither on the choice of the anchor cell, nor on the order in which the two edge cells are added, nor on the order in which interior cells are added.

Each of the elementary cells can be placed into an xy slice with its own distinct characteristic probability, say π_i , $i = 1, \dots, x_1 x_2$. Except for the anchor cell, all elementary probabilities π_i are conditional ones, since the availability of a free site for a given cell depends not only on the number of obstacles in the slice due to j plates already present in the system, but also on the presence of the previously placed cells of the test plate. The expected number of locations ν_{j+1} accessible to the test plate will thus be the product of these probabilities:

$$\frac{\nu_{j+1}}{n_0} = \pi_1 \prod_{i=2}^{x_1 x_2} \pi_i. \quad (5)$$

The probability that a given site in the xy slice is free for the anchor cell is simply given by the volume fraction of free sites in the system [2,8,14]:

$$\pi_1 = \frac{n_0 - j x_1 x_2}{n_0}. \quad (6)$$

For the remaining cells, the conditional probability of finding a free space for a particular cell is given by the volume fraction of empty sites in a solution of the empty sites and of the effective obstacles to the cell resulting from all j plates of the system, $\sum_{k=1}^j K_i^k$, the particular type and number of obstacles K_i^k being characteristic for each of the cells [2,14]:

$$\pi_i \approx \frac{n_0 - j x_1 x_2}{n_0 - j x_1 x_2 + \sum_{k=1}^j K_i^k}. \quad (7)$$

Note that Eq. (7) disregards the presence of previously placed cells of the $j+1$ plate; it has been argued in the past [8,14] that accounting for these cells has no effect on the final form of Z_{comb} within the approximations adopted in the lattice method.

Our task is then to evaluate the number of obstacles for each cell of the test plate. As argued for rodlike particles by Flory [5] and Warner [8], the number of obstacles can be expressed via projections of the system particles onto a particular reference plane. In the Flory laboratory frame approach, this is a plane perpendicular to the nematic director, while in the Warner molecular frame approach it is a plane transverse to the rod. Wnek and Moscicki [14] have shown that for the disk system in the former approach, the relevant planes are two mutually orthogonal planes parallel to the nematic director. For the present theory it is sufficient to know the projections of a given plate of the system, say the k th, onto three planes of the $\{xyz\}$ lattice: two principal planes ϕ_{xz}^k and ϕ_{yz}^k , and a plane perpendicular to the plate diagonal, ϕ_{qz}^k , in order to be able to evaluate the number of obstacles the k th plate can impose on the construction of the test plate.

After placing the anchor cell, we add one by one two adjacent edge cells; cf. Fig. 2. Let the first of the two be positioned along the x_1 edge. From simple geometrical considerations, one finds that any given k th plate of the system,

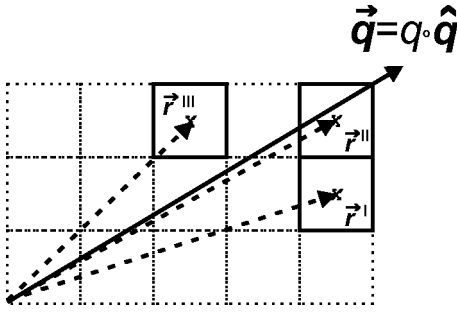


FIG. 3. Placing the interior cells: their radial vectors and the plate diagonal vector (see text for details).

due to its translational freedom along the y axis, can obstruct the placement of the cell in n_y ways, each of them statistically weighted by the local Warner steric constraint, $p_{yz}^k(n_y)$, where locality is emphasized by the n_y argument. The total number of possible obstacles for the k th plate is then the weighted sum of all contributions,

$$K_{e1}^k = \sum_{n_y} p_{yz}^k(n_y) = \phi_{yz}^k, \quad (8)$$

i.e., it is equal to the projection of the k th plate onto the yz plane, ϕ_{yz}^k . By identical arguments, the total number of obstacles for the edge cell along x_2 is the projection of the k th plate onto the xz plane, ϕ_{xz}^k :

$$K_{e2}^k = \sum_{n_x} p_{xz}^k(n_x) = \phi_{xz}^k. \quad (9)$$

Clearly, the results in Eqs. (8) and (9) are independent of each other, and thus independent of the order in which the edge cells are located on the lattice.

Let us next consider the number of ways the k th plate can block an interior cell in Fig. 2. The blocking results from the translational freedom of the k th plate perpendicular to the direction in which the interior cell is added, i.e., transverse to the cell radial vector (with respect to the anchor cell) \mathbf{r} (see Fig. 3). By analogous arguments as for the previous two cells, the total number of obstacles is

$$K_q^k = \sum_{n_q} p_{qz}^k(n_q) = \phi_{qz}^k, \quad (10)$$

where ϕ_{qz}^k is the projection of the k th plate onto the plane normal to \mathbf{r} .

We proceed further by adding the next pair of edge cells, thus completing the construction front line (cf. Fig. 2). The addition of any adjacent row to the construction boundary proceeds along the same scheme: first the interior cells, then the edge cells. From inspection of Fig. 2 it follows that the number of obstacles to all edge cells is given by either Eq. (8) or Eq. (9). The number of obstacles to the interior cells will vary from cell to cell, since their radial vectors are not collinear; cf. Fig. 3. However, as argued in [14], this variation is not very broad. Each interior cell can then be assigned some mean value with only a minor effect on the final result. For simplicity and clearness we select the value to be equal to K_q^k corresponding to the unit vector $\hat{\mathbf{r}}$ along the plate di-

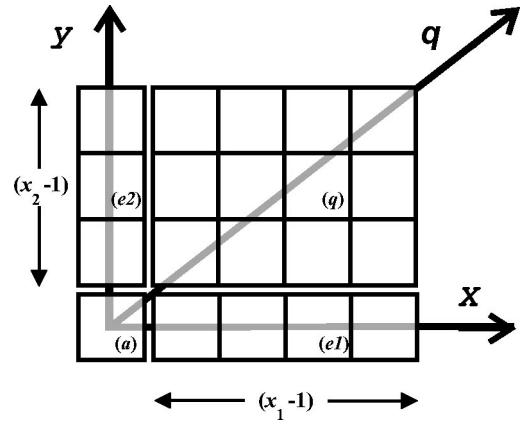


FIG. 4. Four categories of the test plate cells in terms of their statistical similarity.

agonal, $\hat{\mathbf{r}} \equiv \hat{\mathbf{q}}$; cf. Fig. 3. It is identical with the statistical mean for a square plate and slightly different from the latter for rectangular plates.

The cells of the test plate thus divide into four categories in terms of their statistical similarity (see Fig. 4). The single member category, denoted in what follows by the subscript a , constitutes the anchor cell. To the other two categories, which are identified by subscripts $e1$ and $e2$, belong the edge cells along x_1 and x_2 , and there are $(x_1 - 1)$ and $(x_2 - 1)$ of each of them in the plate. The remaining $(x_1 - 1)(x_2 - 1)$ cells form yet another category, the *interior cell* category, which we denote by the subscript q .

This leads to a substantial simplification of Eq. (5):

$$\frac{\nu_{j+1}}{n_0} = \pi_a \pi_{e1}^{x_1-1} \pi_{e2}^{x_2-1} \pi_q^{(x_1-1)(x_2-1)}, \quad (11)$$

with π_i , $i \equiv a, e1, e2, q$, given, respectively, by Eqs. (6) and (7), where the relevant K_i^k are estimated in Eqs. (8), (9), and (10).

The number of obstacles for a cell of the i category, $\sum_{k=1}^j K_i^k$, depends on the orientational distribution of the system plates, so that an exact calculation of that number is expected to be cumbersome and the final expression unwieldy. In the spirit of the lattice method approximation we introduce, therefore, a number of simplifications, which yield an approximate number of obstacles that has a simple dependence on the basic parameters of the system while at the same time keeping the error thus introduced in the evaluation of the partition function to a minimum. In particular, we benefit from the fact that each plate of the system in equilibrium should on average contribute the same amount of obstacles to every xy slice of the system. In other words, our system is, in this treatment, thermodynamically equivalent to a system of j plates, each with the same (mean) orientational order. At no expense to the completeness of the theory, we can use the mean values of the basic parameters of the system in what follows in place of summations over the system:

$$\sum_{k=1}^j K_i^k = j \bar{K}_i = j \bar{\phi}_i, \quad (12)$$

so that Eq. (7) becomes simply

$$\pi_i \approx \frac{n_0 - jx_1x_2}{n_0 - jx_1x_2 + j\bar{\varphi}_i}, \quad (13)$$

where $\bar{\varphi}_i$, $i \equiv e1, e2$, or q , is the plate mean projection onto the relevant plane, averaged over the equilibrium orientational distribution function of the system.

The projection area of a randomly selected k th plate onto the yz and xz planes can be expressed with the aid of the relevant Euler angles [cf. Eq. (1) and Appendix A] as

$$\begin{aligned} \varphi_{e1}^k &= \varphi_{yz}^k = x_1x_2|\cos \alpha^k \sin \beta^k| + x_1|\sin \alpha^k \cos \gamma^k \\ &\quad + \cos \alpha^k \cos \beta^k \sin \gamma^k| \\ &\quad + x_2|\cos \alpha^k \cos \beta^k \cos \gamma^k - \sin \alpha^k \sin \gamma^k| \end{aligned} \quad (14)$$

$$= x_1x_2|\rho_{13}^{\Omega, \Omega'}| + x_1|\rho_{12}^{\Omega, \Omega'}| + x_2|\rho_{11}^{\Omega, \Omega'}| \equiv \varphi_{e1}^k(\Omega, \Omega'), \quad (15)$$

$$\begin{aligned} \varphi_{e2}^k &\equiv \varphi_{xz}^k = x_1x_2|\sin \alpha^k \sin \beta^k| + x_1|\cos \alpha^k \cos \gamma^k \\ &\quad - \sin \alpha^k \cos \beta^k \sin \gamma^k| + x_2|\sin \alpha^k \cos \beta^k \cos \gamma^k \\ &\quad + \cos \alpha^k \sin \gamma^k| \end{aligned} \quad (16)$$

$$= x_1x_2|\rho_{23}^{\Omega, \Omega'}| + x_1|\rho_{22}^{\Omega, \Omega'}| + x_2|\rho_{21}^{\Omega, \Omega'}| \equiv \varphi_{e2}^k(\Omega, \Omega'), \quad (17)$$

and the projection onto the plane orthogonal to the diagonal is

$$\begin{aligned} \varphi_q^k &\equiv \varphi_{qz}^k = x_1x_2|\cos(\alpha^k - \phi) \sin \beta^k| + x_1|\sin(\alpha^k - \phi) \cos \gamma^k \\ &\quad + \cos(\alpha^k - \phi) \cos \beta^k \sin \gamma^k| + x_2|\cos(\alpha^k - \phi) \\ &\quad \times \cos \beta^k \cos \gamma^k - \sin(\alpha^k - \phi) \sin \gamma^k| \end{aligned} \quad (18)$$

$$= x_1x_2|\rho_{13}^{\Omega, \Omega''}| + x_1|\rho_{12}^{\Omega, \Omega''}| + x_2|\rho_{11}^{\Omega, \Omega''}| \equiv \varphi_q^k(\Omega, \Omega''), \quad (19)$$

where Ω'' denotes an auxiliary set of angles, $\Omega'' \equiv (\alpha' - \phi, \beta', \gamma')$, ϕ being the angle between the test plate diagonal and its $e1$ edge:

$$\cos \phi = \frac{x_1}{\sqrt{x_1^2 + x_2^2}}. \quad (20)$$

A few comments are necessary at this point. For highly asymmetric molecules, i.e., when $x_1 \gg 1$ and $x_2 \gg 1$, small effects from a plate of small finite thickness (~ 1) can be neglected, and the last two terms in the right-hand side (RHS) of Eqs. (14)–(19) can be approximated by a constant. However, when either $x_1 \approx 1$ or $x_2 \approx 1$, which corresponds to a convergence of the plates to the rod limit, one of these two RHS terms becomes comparable to the first RHS term and cannot be neglected. Once the formalism for the general case is outlined, we will address both limiting cases in Appendixes B and C.

Calculation of the mean projection of the system plates onto the planes xz , yz , and qz requires double averaging of Eqs. (14)–(19). First, we have to average φ_i^k over the equi-

librium orientation distribution function of the system plates, $w_{x_1x_2}(\Omega') = n_{\Omega'} / n_x$. Second, the test plate is being inserted into the system at random, and therefore the orientation of $\{xyz\}$ must also be averaged over the orientation distribution function of the $(j+1)$ th plate, $w_{x_1x_2}(\Omega) = n_{\Omega} / n_x$. Since the test plate is inserted into the system in such a way that it does not change the equilibrium parameters, the functional forms of $w_{x_1x_2}(\Omega)$ and $w_{x_1x_2}(\Omega')$ are the same. This distinction barely reflects the order of taking the average, which is important for the final result. Note also that the subscript “ x_1x_2 ” on w refers to the important dimensions of the solute particle; for a square plate it will be xx , and either $1x$, $x1$, or z for a rodlike solute; cf. Appendixes B and C.

Thus, the mean projections of interest can be formally written as

$$\bar{\varphi}_i = \int \int w_{x_1x_2}(\Omega) w_{x_1x_2}(\Omega') \varphi_i^k(\Omega, \Omega') d\Omega d\Omega',$$

$$i = e1, e2,$$

$$\bar{\varphi}_q = \int \int w_{x_1x_2}(\Omega) w_{x_1x_2}(\Omega'') \varphi_q^k(\Omega, \Omega'') d\Omega d\Omega'', \quad (21)$$

where $\int_{\Omega} w_{x_1x_2}(\Omega) d\Omega = 1$. Note that the need to use the molecular frame ends at this point, since from now on all calculations are performed in the laboratory coordinate frame.

Equations (21) are integrable in a straightforward way for the limiting cases of the isotropic state and of the perfectly ordered state. In the isotropic phase, the distribution of plate orientations is uniform over the whole solid angle, the distribution function does not depend on the coordinate system, and therefore the average projections are equal to each other:

$$\bar{\varphi}_x^l = (x_1 + x_2 + x_1x_2)/2. \quad (22)$$

Note that the average projection in the isotropic phase is larger than the plate lid area, due to the finite plate thickness, whose contribution is not negligible in that phase.

In the perfect order case (tiling problem [19]), all relevant reference frames coincide, and the average projections become

$$\bar{\varphi}_{e1} = x_2,$$

$$\bar{\varphi}_{e2} = x_1,$$

$$(23)$$

$$\bar{\varphi}_q = 2x_1x_2(x_1^2 + x_2^2)^{-1/2}.$$

In the course of further development of the general treatment some simplifying approximations are necessary. However, in doing so we will make choices that ensure that both limiting results in Eqs. (22) and (23) are always recovered.

The equilibrium orientation distribution function $w_{x_1x_2}(\Omega)$ in Eqs. (21) should minimize the Gibbs function. Clearly, G depends on the distribution function in a complex manner, and the differentiation in Eq. (2) involves $w_{x_1x_2}(\Omega)$ both directly and indirectly through the average projections $\bar{\varphi}_i$, $i \equiv e1, e2$, and q . Auxiliary functional derivatives involved in the differentiation are

$$n_x \frac{\partial \bar{\varphi}_i}{\partial n_\Omega} = \int w_{x_1 x_2}(\Omega') [\varphi_i^k(\Omega, \Omega') + \varphi_i^k(\Omega', \Omega)] d\Omega' \equiv \mathcal{Q}_i,$$

$$n_x \frac{\partial \bar{\varphi}_q}{\partial n_\Omega} = \int w_{x_1 x_2}(\Omega') [\varphi_q^k(\Omega, \Omega'') + \varphi_q^k(\Omega'', \Omega)] d\Omega' \equiv \mathcal{Q}_q, \quad (24)$$

where $i = e1, e2$, and the appearance of $\varphi_i^k(\Omega', \Omega)$ and $\varphi_j^k(\Omega'', \Omega)$ results from taking partial derivatives over Ω and Ω' and then benefiting from the equivalence of the functional forms of $w_{x_1 x_2}(\Omega')$ and $w_{x_1 x_2}(\Omega)$.

The distribution minimizing G has the general form

$$w_{x_1 x_2}(\Omega) = \frac{n_\Omega}{n_x} = f_1^{-1} \sin \beta \exp\left(-\sum_i b_i \mathcal{Q}_i\right), \quad i = e1, e2, q, \quad (25)$$

where $f_1 = \int d\alpha d\beta d\gamma \sin \beta \exp(-\sum_i b_i \mathcal{Q}_i)$, and the b_i 's are given by

$$\begin{aligned} b_{e1} &= \frac{(x_1 - 1)x_1 x_2}{(x_1 x_2 - \bar{\varphi}_{e1})^2} \\ &\quad \times \left\{ -v_x^{-1} \ln \left[1 - v_x \left(1 - \frac{\bar{\varphi}_{e1}}{x_1 x_2} \right) \right] - 1 + \frac{\bar{\varphi}_{e1}}{x_1 x_2} \right\}, \\ b_{e2} &= \frac{(x_2 - 1)x_2 x_1}{(x_1 x_2 - \bar{\varphi}_{e2})^2} \\ &\quad \times \left\{ -v_x^{-1} \ln \left[1 - v_x \left(1 - \frac{\bar{\varphi}_{e2}}{x_1 x_2} \right) \right] - 1 + \frac{\bar{\varphi}_{e2}}{x_1 x_2} \right\}, \\ b_q &= \frac{(x_1 - 1)(x_2 - 1)x_1 x_2}{(x_1 x_2 - \bar{\varphi}_q)^2} \\ &\quad \times \left\{ -v_x^{-1} \ln \left[1 - v_x \left(1 - \frac{\bar{\varphi}_q}{x_1 x_2} \right) \right] - 1 + \frac{\bar{\varphi}_q}{x_1 x_2} \right\}, \end{aligned} \quad (26)$$

where $v_x = x_1 x_2 n_x / n_0$ is the (volume) fraction of plates in the system.

The self-consistency of the model requires simultaneous fulfillment of Eqs. (21), (24)–(26). This is not solvable analytically, and has to be established numerically, independently for each desired size of the solute particle. Two limiting cases of the particle size are of particular interest for their relevance to the most frequently encountered situation in real systems, which we will address later in the paper.

Once the mean projections in equilibrium are known, one can calculate the configurational part of the partition function, Z_{comb} [cf. Eq. (11)],

$$\begin{aligned} Z_{\text{comb}} &= \frac{1}{n_x!} \prod_{j=1}^{n_x} \nu_{j+1} = \frac{1}{n_x!} \prod_{j=1}^{n_x} (n_0 - j x_1 x_2)^{x_1 x_2} \\ &\quad \times (n_0 - j x_1 x_2 + j \bar{\varphi}_{e1})^{-(x_1 - 1)} \\ &\quad \times (n_0 - j x_1 x_2 + j \bar{\varphi}_{e2})^{-(x_2 - 1)} \\ &\quad \times (n_0 - j x_1 x_2 + j \bar{\varphi}_q)^{-(x_1 - 1)(x_2 - 1)}. \end{aligned} \quad (27)$$

Application of the usual methods of manipulating Z_{comb} into a more tractable form, e.g., Eq. (23) of Ref. [14], and Stirling's approximations for the factorials yields

$$\begin{aligned} -\ln(Z_{\text{comb}}) &= n_x \ln \frac{n_x}{n_0} + n_s \ln \frac{n_s}{n_0} - \frac{(x_1 - 1)}{x_1 x_2 - \bar{\varphi}_{e1}} (n_s + n_x \bar{\varphi}_{e1}) \\ &\quad \times \ln \left[1 - v_x \left(1 - \frac{\bar{\varphi}_{e1}}{x_1 x_2} \right) \right] \\ &\quad - \frac{(x_2 - 1)}{x_1 x_2 - \bar{\varphi}_{e2}} (n_s + n_x \bar{\varphi}_{e2}) \\ &\quad \times \ln \left[1 - v_x \left(1 - \frac{\bar{\varphi}_{e2}}{x_1 x_2} \right) \right] - \frac{(x_1 - 1)(x_2 - 1)}{x_1 x_2 - \bar{\varphi}_q} \\ &\quad \times (n_s + n_x \bar{\varphi}_q) \ln \left[1 - v_x \left(1 - \frac{\bar{\varphi}_q}{x_1 x_2} \right) \right]. \end{aligned} \quad (28)$$

To complete the steric contribution to the Gibbs function of the system, we need the orientational part of the partition function, Z_{or} . It is customary for the lattice methods to use [2,6,8,14]

$$-\ln(Z_{\text{or}}) = -\sum_{\Omega} n_{\Omega} \left(\sigma \omega_{\Omega} \frac{n_x}{n_{\Omega}} \right), \quad (29)$$

where σ is an arbitrary constant close to unity and ω_{Ω} is a measure of the solid angle and is equal to $\sin \beta$, in terms of the relevant Euler angles.

The Gibbs function of the anisotropic phase (A) thus becomes

$$\begin{aligned} \frac{G^A}{n_0 k_B T} &= \frac{v_x^A}{x_1 x_2} \ln \frac{v_x^A}{x_1 x_2} + (1 - v_x^A) \ln(1 - v_x^A) \\ &\quad - \frac{v_x^A}{x_1 x_2} \ln f_1 - \frac{(x_1 - 1)}{x_1 x_2 - \bar{\varphi}_{e1}} \left[1 - v_x^A \left(1 - \frac{\bar{\varphi}_{e1}}{x_1 x_2} \right) \right] \\ &\quad \times \ln \left[1 - v_x^A \left(1 - \frac{\bar{\varphi}_{e1}}{x_1 x_2} \right) \right] - \frac{(x_2 - 1)}{x_1 x_2 - \bar{\varphi}_{e2}} \\ &\quad \times \left[1 - v_x^A \left(1 - \frac{\bar{\varphi}_{e2}}{x_1 x_2} \right) \right] \\ &\quad \times \ln \left[1 - v_x^A \left(1 - \frac{\bar{\varphi}_{e2}}{x_1 x_2} \right) \right] - \frac{(x_1 - 1)(x_2 - 1)}{x_1 x_2 - \bar{\varphi}_q} \\ &\quad \times \left[1 - v_x^A \left(1 - \frac{\bar{\varphi}_q}{x_1 x_2} \right) \right] \\ &\quad \times \ln \left[1 - v_x^A \left(1 - \frac{\bar{\varphi}_q}{x_1 x_2} \right) \right] - 2 \frac{v_x^A}{x_1 x_2} \\ &\quad \times [b_{e1} \bar{\varphi}_{e1} + b_{e2} \bar{\varphi}_{e2} + b_q \bar{\varphi}_q], \end{aligned} \quad (30)$$

where the first two terms on the RHS are the expected ideal mixing terms. Their presence is a direct consequence of accounting for the plate interior cells by the present model (cf. Fig. 4).

The chemical potentials in the anisotropic phase take the form

$$\begin{aligned} \frac{\mu_s^A}{k_B T} = & \ln(1 - v_x^A) - \frac{(x_1 - 1)}{x_1 x_2 - \bar{\varphi}_{e1}} \ln \left[1 - v_x^A \left(1 - \frac{\bar{\varphi}_{e1}}{x_1 x_2} \right) \right] \\ & - \frac{(x_2 - 1)}{x_1 x_2 - \bar{\varphi}_{e2}} \ln \left[1 - v_x^A \left(1 - \frac{\bar{\varphi}_{e2}}{x_1 x_2} \right) \right] \\ & - \frac{(x_1 - 1)(x_2 - 1)}{x_1 x_2 - \bar{\varphi}_q} \ln \left[1 - v_x^A \left(1 - \frac{\bar{\varphi}_q}{x_1 x_2} \right) \right] \end{aligned} \quad (31)$$

and

$$\begin{aligned} \frac{\mu_x^A}{k_B T} = & \ln \frac{v_x^a}{x_1 x_2} - \ln f_1 + \frac{(x_1 - 1)}{x_1 x_2 - \bar{\varphi}_{e1}} \bar{\varphi}_{e1} \\ & \times \left\{ \left(\frac{2x_1 x_2}{(x_1 x_2 - \bar{\varphi}_{e1}) v_x^A} - 1 \right) \right. \\ & \times \ln \left[1 - v_x^A \left(1 - \frac{\bar{\varphi}_{e1}}{x_1 x_2} \right) \right] + 2 \left. \right\} + \frac{(x_2 - 1)}{x_1 x_2 - \bar{\varphi}_{e2}} \bar{\varphi}_{e2} \\ & \times \left\{ \left(\frac{2x_1 x_2}{(x_1 x_2 - \bar{\varphi}_{e2}) v_x^A} - 1 \right) \ln \left[1 - v_x^A \left(1 - \frac{\bar{\varphi}_{e2}}{x_1 x_2} \right) \right] + 2 \right\} \\ & + \frac{(x_1 - 1)(x_2 - 1)}{x_1 x_2 - \bar{\varphi}_q} \bar{\varphi}_q \times \left\{ \left(\frac{2x_1 x_2}{(x_1 x_2 - \bar{\varphi}_q) v_x^A} - 1 \right) \right. \\ & \left. \times \ln \left[1 - v_x^A \left(1 - \frac{\bar{\varphi}_q}{x_1 x_2} \right) \right] + 2 \right\}. \end{aligned} \quad (32)$$

B. The isotropic phase

A uniform density of the orientation distribution function n_Ω/n_x over the whole solid angle in the isotropic phase obviously cancels out Z_{or} . For symmetry reasons all relevant average projections are equal to each other and given by Eq. (22), and the Gibbs function becomes

$$\begin{aligned} \frac{G^I}{n_\Omega k_B T} = & \frac{v_x^I}{x_1 x_2} \ln \frac{v_x^I}{x_1 x_2} + (1 - v_x^I) \ln(1 - v_x^I) - \frac{(x_1 x_2 - 1)}{x_1 x_2 - \bar{\varphi}_x^I} \\ & \times \left[1 - v_x^I \left(1 - \frac{\bar{\varphi}_x^I}{x_1 x_2} \right) \right] \ln \left[1 - v_x^I \left(1 - \frac{\bar{\varphi}_x^I}{x_1 x_2} \right) \right]. \end{aligned} \quad (33)$$

The chemical potentials in the isotropic phase are

$$\frac{\mu_s^I}{k_B T} = \ln(1 - v_x^I) - \frac{(x_1 x_2 - 1)}{x_1 x_2 - \bar{\varphi}_x^I} \ln \left[1 - v_x^I \left(1 - \frac{\bar{\varphi}_x^I}{x_1 x_2} \right) \right], \quad (34)$$

$$\frac{\mu_x^I}{k_B T} = \ln \frac{v_x^I}{x_1 x_2} - \frac{(x_1 x_2 - 1)}{x_1 x_2 - \bar{\varphi}_x^I} \bar{\varphi}_x^I \ln \left[1 - v_x^I \left(1 - \frac{\bar{\varphi}_x^I}{x_1 x_2} \right) \right]. \quad (35)$$

This completes the basic theoretical considerations of the paper. We may now proceed to some illustrative calculations, in particular, the uniaxial particle limit, i.e., uniaxial disks on the one hand and rods on the other. This offers us the possibility of testing the correctness of the theory in the light of existing data from the literature.

III. CALCULATIONS AND DISCUSSION

The self-consistency of Eqs. (21), (24)–(26) minimizes the free energy, thus ensuring the equilibrium of the system. However, the self-consistency condition is not solvable analytically, and requires a numerical treatment. Because of the complexity of the formalism, convergence of the numerical procedure for the general case is a significant problem and exploring it in detail is beyond the scope of this paper [20]. Instead, we concentrate on two limiting cases, i.e., those of (i) uniaxial disks and (ii) rods (see Appendixes B and C, respectively). Such a selection is dictated not only by the fact that the thermodynamic properties of the two systems have been extensively studied in the past [1–4,6,8,10,11,14,17,23–30], so that predictions of our model can be critically tested, but also because there is available an iterative algorithm, which is highly convergent for a somewhat similar but simpler self-consistency problem studied by Herzfeld, Berger, and Wingate [31]. In a particularly critical test of this algorithm we verified that, when applied to the theory of Warner [8] for rods, it recovers Warner's results to within 0.2%.

As it turns out, the efficiency of the algorithm in finding the equilibrium parameters depends strongly on the initial guess for the distribution function [31]. This effect is clearly visible, e.g., when searching for the threshold (minimum) aspect ratio sufficient for existence of a stable anisotropic phase in the pure system ($v_x = 1$); on increasing the particle anisotropy the onset of the anisotropic phase at some threshold aspect ratio should be marked by, first, the existence of a nontrivial (anisotropic) distribution function and, second, the coexistence of the anisotropic and isotropic phases, $G^A = G^I$. In general, for any reasonable guess function, the equilibrium orientational distribution in the anisotropic phase can be found even for a particle anisotropy slightly below the threshold one. However, we found by a trial-and-error method that the guess functions divide naturally into three categories, roughly speaking those of a small, medium, and large width at half maximum (FWHM). For functions with a small FWHM, the minimum critical particle anisotropy for the formation of the anisotropic phase can be found, but the phase is unstable since $G^A > G^I$. Only on increasing the aspect ratio further does the free energy of the anisotropic phase decrease and become, at some point, equal to that of the isotropic phase. Broadening the guess distribution above some width marks the onset of the second category of functions for which the same threshold particle anisotropy and the same lowest (“global”) free energy minimum, i.e., the same stable results for n_Ω/n_x , $\bar{\varphi}_i$, and Q_i , $i = e1, e2, q$, are always obtained. Characteristically, the threshold aspect ratio is the same for the former and latter categories of the trial functions. However, the algorithm cannot recover the anisotropic phase parameters at the threshold aspect ratio if the trial function becomes too broad, which always leads to $G^A \neq G^I$ (third category). From the practical point of view, we considered a class of trial functions adequate for our purposes if the algorithm converged at the threshold anisotropy and the system parameters characteristic for the anisotropic-isotropic phase transition. Examples of such simple useful guess distribution functions applied in this work are given in Appendix D.

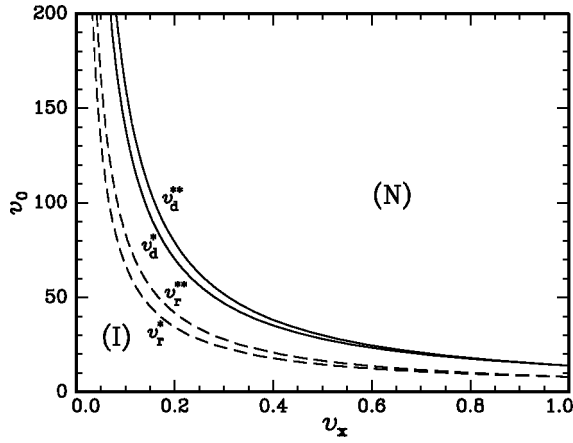


FIG. 5. Volume concentrations of phases in equilibrium, v_x , as a function of the molecular volume v_0 for (dashed lines) rods and (solid lines) square boards. *I* and *N* denote the isotropic and nematic phases, respectively. Critical concentrations v_x^* and v_x^{**} set the boundaries of the coexistence range *I*+*N*. Molecular volume in lattice units.

Typically, we first examined the properties of the pure systems ($v_x = 1$). For each system on varying x a phase transition is found at some critical threshold value x^{crit} , below which particles are always disordered and above always ordered (nematic). We calculated $x_d^{\text{crit}} \equiv x^{\text{crit}} \approx 3.742$ and $\bar{\phi}_d^{\text{crit}} \approx 8.249$ for disks, and $x_r^{\text{crit}} \equiv x^{\text{crit}} \approx 8.019$ and $\bar{\phi}_r^{\text{crit}} \approx 4.627$ for rods.

Next, the properties of each system on dilution are studied. For any given aspect ratio greater than x^{crit} we always found a biphasic range of concentrations where the isotropic and nematic phases coexisted. The low v_x^* and high v_x^{**} concentration boundaries of the biphasic range were found by solving the simultaneous equations for the chemical potentials, Eq. (3), for a given aspect ratio x and varying the composition of the mixture. There are two possible ways of presenting the calculated phase diagrams. A plot of the solute volume fraction vs particle volume (v_x, v_0) is more adequate for lyotropic systems, while a plot of the volume fraction vs aspect ratio (v_x, x) is usually used when discussing thermotropic systems. The choice is arbitrary but since the present theory works better the larger the aspect ratio (e.g., stiff, rodlike polymers, colloids), we decided to use the former (cf. Fig. 5). It should be noted that for every solute for any given particle volume (or aspect ratio), on traversing the biphasic range, the equilibrium parameters of the nematic phase remain constant and have the threshold (minimum) values characteristic of the first occurrence of the stable nematic phase. The only variable moving the system across the biphasic range is the relative volume participation of the isotropic and nematic phases in the biphasic material. The parameters of particular importance are the equilibrium value of the nematic order parameter $S = P_2(\cos^2 \beta)$, and the volume fraction (or density) jump δv_x at the transition. In Fig. 6 variation of both parameters along the boundaries is shown as a function of the normalized molecular volume v_0/v_0^{crit} where $v_0 = x \times x$ or x , and $v_0^{\text{crit}} = x_d^{\text{crit}} \times x_d^{\text{crit}}$ or x_r^{crit} , for disks and rods, respectively.

Since this work develops Warner's idea of the molecular frame lattice [8] to a quite general case of platelike particles,

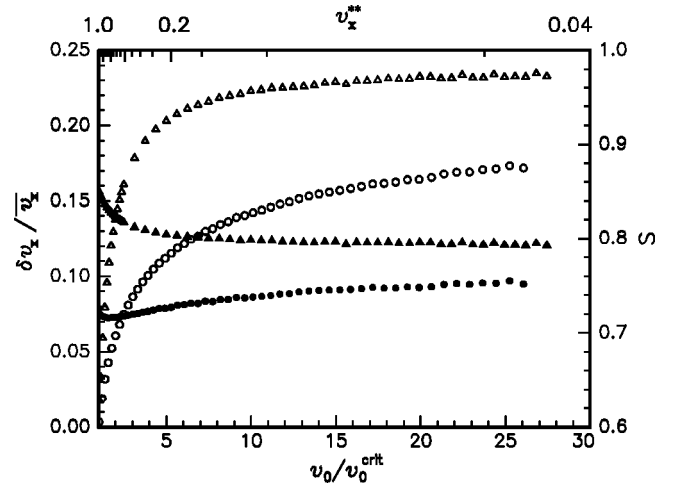


FIG. 6. The isotropic-nematic phase transition in (triangles) rod-like and (circles) square boardlike systems. Open symbols, RHS, volume concentration (density) change normalized to the mean concentration of the system, $\delta v_x / \bar{v}_x$, and full symbols, LHS, the nematic order parameter S as a function of the molecular volume normalized to the critical molecular volume v_0/v_0^{crit} (bottom) and the nematic phase concentration v_x^{**} (top).

his numerical data serve us as a natural reference for testing our numerical results in the rodlike limit. A basic observation is that in a pure system and in solution our nematic phase appears at somewhat lower threshold rod length and is slightly more orientationally ordered than that of Warner [8], e.g., compare our $x_r^{\text{crit}} = 8.019$ with his 8.9832, and $S = 0.85$ vs 0.8314, respectively. The phase diagrams are very much alike in shape and extent but clearly they do not overlap. Our phase diagram is consistently below Warner's (see Fig. 7), i.e., it is shifted a little bit toward lower concentrations and aspect ratios. Such differences are expected. From inspection of both theories it follows that the difference originates in the approximations adopted in [8] [see especially his Eq. (9)], and Eqs. (B2) and (C10), introduced when simplifying the expressions for the particle projections. For long rods, the overwhelming contribution to the projections ϕ_i^k in Eqs. (14)–(19) comes from the rod length, and the approximation

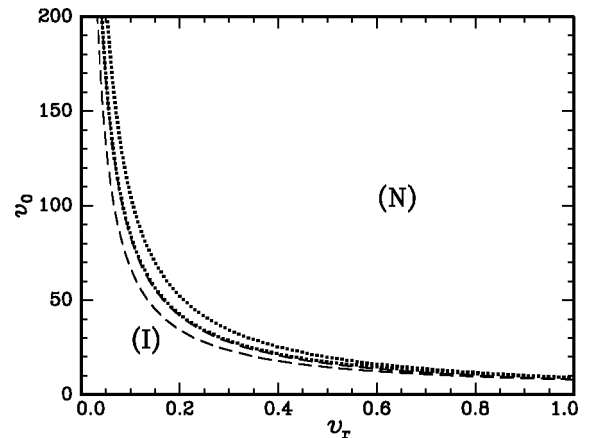


FIG. 7. Rods in solution. Volume concentrations of phases in equilibrium, $v_x \equiv v_r$, as a function of the molecular volume v_0 after Warner [8] (dotted lines), and from the present study (dashed lines). Molecular volume in lattice units.

leaves out the angular dependence of the minor contributions from the rod width, replacing them with some constant factors, in a manner analogous to that of Warner [8]. Similarly, in the boardlike particle limit, contributions from the plate lids dominate the projections and, within the approximations applied, the finite plate thickness is accounted for as a small angle-independent contribution only. Although there is some freedom in assigning particular values to these factors, our results and the results of Warner [8] show that the choice of these values has non-negligible consequences for the phase behavior. There are two limiting cases of orientational order, perfect order and isotropic disorder, for which the distribution function is known and the projections can be calculated exactly. The proper behavior of the approximations in these limits may then be used as a guide to select the correct constant factor. Warner's choice of the constant for the rodlike system is such that it ensures the appropriate behavior of the approximation in the perfect order limit [8]. We believe, however, that the approximations adopted should ensure the proper behavior of the projections not only in the perfect order but *also* in the isotropic disorder limit. For rodlike particles, comparison of our approximation in Eq. (C16) with that of Warner [8] [cf. his Eq. (9)] shows that the difference is in the proportionality factor only. Notably, when we restrict the normalization to the perfect order limit alone, we recover Warner's results. However, such a restriction underestimates the projection magnitude in the isotropic phase and thus it leads to an enhanced stabilization of the isotropic phase (see Fig. 7). On the other end, it somewhat underestimates the orientational entropy of particles substantially disordered in the nematic phase.

As may be expected, in the square board limit the calculated critical minimum value of the aspect ratio, $x_d^{\text{crit}} = 3.742$, is higher than the value 3.015 obtained within the classical laboratory frame approach [14]. The difference parallels the one found when comparing analogously numerical results of the laboratory frame [2,11] and the molecular frame [8] methods applied to rodlike particle systems. By the same arguments as Warner's for rods [8], higher values of x_d^{crit} and lower values of S reflect fewer restrictions in the orientational phase space of the solute particles, i.e., allowance for continuous reorientation of particles, and a much lower entropy penalty for disoriented particles in the nematic phase in the molecular frame approach.

It has been suggested in the past [14] that, when using such a molecular parameter as the molecular volume v_0 , there is a far-reaching symmetry between the (v_x, v_0) phase diagrams calculated by lattice methods for disks and rods. Also, a theory based on the second virial coefficient [29] and a computational work of Frenkel and Mulder [25] suggest a symmetry in the phase diagrams of rods and disks. On the other hand, considerable asymmetry in the thermodynamic properties of fluids of prolate and oblate particles is observed in some computer simulations [32]. The latter is in line with the findings of the present study that quantitative symmetry between the (v_x, v_0) phase diagrams of rod- and disklike systems is not obvious (cf. Fig. 5). Indeed, although there is a visible congruency between the shapes of the biphasic regions of both systems, the phase diagram for rods is consistently shifted toward the origin of the plane, i.e., to much lower concentrations and smaller v_0 's. Therefore, when

comparing solutes of the same particle volume there is clear evidence that the isotropic phase in a solution of rod isomorphs is substantially less favored than in one of plate isomorphs at low concentrations (cf. Fig. 5). In other words, for a certain concentration of mesogenic particles of fixed molecular volume, the former can form a nematic phase, while the latter can still have an isotropic phase. This is reflected in the lower value of the rod critical volume compared to that for disks, $v_r^{\text{crit}} = 8.019 < 14.003 = v_d^{\text{crit}}$, higher ordering in the nematic phase, and a relatively broader biphasic range for rods than for disks (cf. Figs. 5 and 6).

The results in Fig. 5 have profound consequences for a rod-disk complex solvent. First, in solutions of mixtures of rods and disks of the same particle volume, separation of the rodlike component in the form of a calamitic nematic phase at low concentrations would prevent formation of, e.g., the biaxial phase in the system. In fact, such segregation is known from other studies, and can be prevented by the presence of either any kind of disk-rod short-range bonding or equilibrium prolate-oblate conformational shape fluctuations of the particles [33–35]. Secondly, if the monodisperse solvent features a rod-disk conformational transformation with concentration, the appearance of a conformational phase transition should be expected. Note finally that we may look at our results from a more conventional point of view for thermotropic liquid crystallinity, i.e., we may compare properties of solutes of the same aspect ratio. One finds then that in the absence of attractive intermolecular forces square boards (disks) form a stable anisotropic state at a significantly lower aspect ratio than do the rod isomorphs.

The properties of the nematic phase in the biphasic range, and at v_x^{**} in particular, vary significantly with both the molecular volume and concentration (cf. Fig. 6). For the same molecular volume, the volume concentration jump across the biphasic range is always greater for rods than for disks, which is a consequence of the higher orientational order of the nematic phase. The nematic-isotropic concentration difference has an initial sharp increase only to flatten out gradually on increasing the system dilution. The order parameter in the rodlike system drops monotonically on dilution, at first rapidly in the early stages of dilution, to reach a plateau of about 0.8 for a more diluted system. For the disklike system on dilution, the order parameter first decreases slightly to a minimum and then increases toward a plateau at about 0.76. Interestingly, this behavior is somewhat different from that of the laboratory frame method, where a monotonic decrease at higher rates was observed [14]. Finally, note a general decrease in the values of the nematic order parameter S and the density jump for disklike systems by comparison with the results obtained from the laboratory lattice method [14].

When discussing phase diagrams resulting from the present theory, we should necessarily comment on the way we estimate the expected number of locations ν_{j+1} accessible to the test plate, since it has important consequences for the phase equilibrium properties. It is assumed that this number can be expressed via the product of probabilities of finding a free site for each of the test disk constituent cells; cf. Eq. (5) and after. Due to statistical similarities between different disk cells, we simplified the problem by assuming that this product can be evaluated by considering the placement

of only a few types of cells: the anchor (a), edge ($e1$ and $e2$), and interior diagonal (q) cells [cf. Eq. (4)]. This is in contrast to a suggestion by Di Marzio, Yang, and Glotzer, who considered the tiling problem of square tiles and argued that sufficient room for a plate on the lattice should be ensured once the edge cells, i.e., a , $e1$, and $e2$ in Fig. 3, are placed [19]. In order to get more insight into this problem, we performed auxiliary calculations with the diagonal terms removed from the present theory. With this prescription, the critical threshold aspect ratio in the pure system nearly doubled to reach $x_{\text{Di Marzio}}^{\text{crit}} = 6.056$. Consequently, the corresponding biphasic range shows up at much higher v_x and v_0 values. However, the density jump across the biphasic range, $\delta v_x / \bar{v}_x$, remained essentially unchanged by the removal of the diagonal terms, but the nematic order parameter increased toward values characteristic of the rodlike system in Fig. 5. Clearly, elimination of the diagonal cells (q) from the computation softens the steric constraints imposed on the plate, which requires in turn a much higher shape anisotropy of particles in order to stabilize the ordered phase. This, however, contradicts experimental observations, which suggest a much *lower* aspect ratio in discotic systems [36–40]. An additional argument in favor of accounting for the interior cells comes from the fact that only in this way can one secure a thermodynamically correct description of the system, i.e., the presence of the entire ideal mixing entropy term of regular solutions, $n_x \ln(n_x/n_0) + n_s \ln(n_s/n_0)$, and the convergence of the entropy per lattice site to zero on approaching the perfect order limit in a pure system on an infinite lattice [17,18]. We believe, therefore, that the prescription of Ref. [19] is more relevant for describing yet another interesting system of “starlike” or “crosslike” particles (cf. [14]).

Only limited comparison of the present numerical results with relevant experimental and computational data is possible. Numerical equilibrium parameters of our model for the rodlike system do not differ substantially from those of Warner, who discussed his results in detail in light of existing experimental evidence [8]. Since the differences between his and our results are for now beyond experimental verification, we concentrate here on discussing results for disklike systems. In the athermal limit one parameter of particular interest is the critical shape anisotropy of molecules necessary for formation of the nematic phase. Phase equilibria computer simulations for disklike particles interacting via repulsive forces usually yield a very low minimum aspect ratio of $x_d^{\text{crit}} \approx 2.75\text{--}3.0$ [25,41]. These values seem to be somewhat below the results obtained from limited experimental x-ray data, which vary from about 3.2 [38,39] to 6.1 [40] deduced from studies in the columnar and crystalline phases of thermotropic disklike molecules, and close to x_d^{crit} values observed for micelles in lyotropic systems [36,37]. However, this comparison has to be judged with care due to unavoidable problems with exact estimation of the molecular (oblate) aspect ratio. Isolated molecules with fully stretched sidechains, and the same molecules packed into the pure system with sidechains taking different conformations, cannot be treated equivalently. Moreover, the columnar phases to which the available x-ray data refer [40,42] are much more dense than the nematic mesophase. Interpenetration of the sidechains between molecules belonging to adjacent columns prevents realistic determination of the overall molecular di-

mensions and, thus, quantitatively reliable extrapolation of these results to the nematic phase. We can only guess that the diameter of a particular disk becomes larger in the less dense nematic mesophase while the width can, but does not have to, remain approximately constant. Under those circumstances, our critical shape anisotropy $x_d^{\text{crit}} = 3.742$ situates us closer to real systems than computer simulations and the results of Wnek and Moscicki [14]. By analogy to rodlike systems [8], we may also expect that nonthermal contributions, i.e., incorporation of attractive forces, will not affect the threshold shape anisotropy to the extent of moving it below the experimentally observed values.

The molecular frame method is a natural alternative to the method of Herzfeld, where on completion of construction of the reference lattice the lattice unit cell size is reduced to the infinitesimal limit [13]. Thus, the unification of phase equilibrium theory for rodlike and disklike systems by means of lattice models becomes as natural as that derived from computer simulations [23,30,32,41,43–45] or off-lattice theories [26,46–49]. In saying so, we are aware of the limitations of the Flory lattice method, in particular its inability to produce the translationally ordered phase (the smectic phase for rods and the columnar one for disks) in the athermal limit (purely from steric effects). This is due to the fact that in the course of discretization of the real solute particles, orientational steric constraints in three dimensional space are converted into polydispersity of the resulting subsolute in one (rods) or two (plates) dimensional isotropic solution. The assumed translational disorder manifests itself in the lack of correlations between neighboring rows of lattice cells parallel to the orientation axis (rods), or slices of lattice cells perpendicular to the axis (plates), thus *a priori* excluding translationally ordered phases from consideration. If needed, the correlations can be introduced into the model by assuming the existence of more or less artificial density waves in rows (the smectic phase of rods) or slices (the columnar phase of plates).

The athermal theory presented here forms a substrate upon which to build further work on nonthermal, amphitropic [16] systems of plates, and biaxial systems of mono- and polydisperse particles [20]. The simple model of Wnek and Moscicki [14] allowed only the study of a solution of disklike particles in the presence of solute-solvent interactions. A substantial advantage of the present theory is the ease with which any kind of intermolecular interactions between all kinds of particles forming the solution can be introduced and studied. In a forthcoming paper we will report on the consequences of introducing the solute-solute attractive intermolecular interactions for the phase equilibrium properties of the system [20]. We will discuss features of the resulting characteristic “bottleneck” phase diagram (cf., e.g., Fig. 10 of Ref. [14]) in terms of the strength of intermolecular forces between all kinds of particles present in the solution. In further work we are interested in mesophases formed by colloids, supramolecules, and polymers in solution. Their aspect ratios in the rod- and disklike forms are of the order of those of conventional liquid crystalline substances [50]. Although more complicated in shape and subject to more complex interactions, they can be studied within the present model where ordering phenomena are primarily dictated by geometry, excluded volume, flexibility, and spe-

cific inter- and intraparticle interactions [38,51,52]. Lyotropic liquid crystalline systems will be of special interest in the future as they undergo phase transitions with simultaneous change of the supraparticle shape with temperature, concentration [53,54], or pressure.

ACKNOWLEDGMENTS

The authors are indebted to Dr. K. A. Earle and Professor D. J. Photinos for reading the manuscript and for many enlightening suggestions. This work was supported by the Polish State Committee for Scientific Research (KBN) through Grant Nos. 2 P03B 210 08 and 2 P03B 015 17.

APPENDIX A: CALCULATION OF AVERAGE PROJECTIONS

In order to calculate the average projections let us first consider the Euler angles $\Omega \equiv (\alpha, \beta, \gamma)$ specifying rotations

$$M(\Omega) \equiv M(\alpha, \beta, \gamma) = \begin{bmatrix} \cos \alpha \cos \beta \cos \gamma - \sin \alpha \sin \gamma & \sin \alpha \cos \beta \cos \gamma + \cos \alpha \sin \gamma & -\sin \beta \cos \gamma \\ -\cos \alpha \cos \beta \sin \gamma - \sin \alpha \cos \gamma & \cos \alpha \cos \gamma - \sin \alpha \cos \beta \sin \gamma & \sin \beta \sin \gamma \\ \cos \alpha \sin \beta & \sin \alpha \sin \beta & \cos \beta \end{bmatrix}. \quad (\text{A3})$$

For the frames and rotations defined schematically in Eq. (1) we have

$$\begin{aligned} r_i &= \sum_j M_{ij}(\Omega) R_j, \\ r_i^k &= \sum_j M_{ij}(\Omega') R_j, \\ r_i &= \sum_j M_{ij}^{-1}(\Omega^k) r_j^k, \end{aligned} \quad (\text{A4})$$

where r_i^k , r_i , and R_i are the unit vector components in the $\{xyz^k\}$, $\{xyz\}$, and $\{XYZ\}$ frames, respectively.

From Eq. (A4) it follows that

$$M_{ij}^{-1}(\Omega^k) = M_{ji}(\Omega^k) = \sum_{m=1}^3 M_{im}(\Omega) M_{jm}(\Omega') \equiv \rho_{ij}^{\Omega, \Omega'}, \quad (\text{A5})$$

which defines the interrelation between different sets of Euler angles of interest, Ω , Ω' , and Ω^k .

APPENDIX B: SPECIAL CASE OF BOARDLIKE PLATES, $x_1 \gg 1$ AND $x_2 \gg 1$

For highly asymmetric molecules $x_1 \gg 1$ and $x_2 \gg 1$, the projections of the k th plate [cf. Eqs. (14)–(19)], reduce to projections of the plate surface only:

that bring the initial coordinate system into coincidence with the final frame [cf. the scheme in Eq. (1)]. If by $M(\Omega)$ we identify the Euler matrix whose elements are calculated from the Euler angles, then a vector whose components in the former are given by $\mathbf{r} \equiv [r_1, r_2, r_3]$ will be given in the latter frame by $\mathbf{r}' \equiv [r'_1, r'_2, r'_3]$ [21]:

$$\mathbf{r}' = M(\Omega) \mathbf{r}, \quad (\text{A1})$$

or

$$r'_i = \sum_j M_{ij}(\Omega) r_j, \quad i, j = 1, 2, 3, \quad (\text{A2})$$

where $M_{ij}(\Omega)$ are elements of the rotation matrix, $M(\Omega)$:

$$\begin{aligned} \phi_{e1}^k(\Omega, \Omega') &\approx x_1 x_2 |\rho_{13}^{\Omega, \Omega'}|, \\ \phi_{e2}^k(\Omega, \Omega') &\approx x_1 x_2 |\rho_{23}^{\Omega, \Omega'}|, \\ \phi_q^k(\Omega, \Omega'') &\approx x_1 x_2 |\rho_{13}^{\Omega, \Omega''}|. \end{aligned} \quad (\text{B1})$$

In order to preserve the limiting behavior in Eqs. (22) and (23), it is necessary to slightly adjust Eq. (B1):

$$\begin{aligned} \phi_{e1}^k(\Omega, \Omega') &\approx x_2 \left[\left(x_1 - 1 + \frac{x_1}{x_2} \right) |\rho_{13}^{\Omega, \Omega'}| + 1 \right], \\ \phi_{e2}^k(\Omega, \Omega') &\approx x_1 \left[\left(x_2 - 1 + \frac{x_2}{x_1} \right) |\rho_{23}^{\Omega, \Omega'}| + 1 \right], \end{aligned} \quad (\text{B2})$$

$$\begin{aligned} \phi_q^k(\Omega, \Omega'') &\approx \frac{2x_1 x_2}{\sqrt{x_1^2 + x_2^2}} \\ &\times \left\{ \left[\frac{\sqrt{x_1^2 + x_2^2}}{2} \left(1 + \frac{x_1 + x_2}{x_1 x_2} \right) - 2 \right] |\rho_{13}^{\Omega, \Omega''}| + 1 \right\}. \end{aligned}$$

It is easily verified that such a modification turns out to be a minor approximation which does not alter the equilibrium parameters of the system in any significant way. Note that the formalism of the isotropic phase remains unaltered by the limit, so Eq. (22) holds.

Uniaxial disks

The formalism simplifies even further if the plates are square, $x_1 = x_2 = x$, i.e., disks. The orientational distribution becomes uniaxial with respect to the discotic nematic director, $\hat{\mathbf{n}} \parallel Z$, depending solely on the Euler angle β :

$$w_{xx}(\Omega) = \frac{n_\Omega}{n_d} \equiv \frac{n_\beta}{n_d} \equiv w_{xx}(\beta), \quad (\text{B3})$$

$$\mathcal{R} = \pi^{-2} \int_0^\pi \int_0^\pi \int_0^{2\pi} \sqrt{1 - [\cos \beta \cos \beta' + \sin \beta \sin \beta' \cos(\alpha - \alpha')]^2} w_{xx}(\beta) w_{xx}(\beta') d(\alpha - \alpha') d\beta d\beta'. \quad (\text{B5})$$

The orientational distribution function is now

$$w_{xx}(\beta) = \frac{\sin \beta \exp(-\sum_i b_i Q_i)}{\int \sin \beta \exp(-\sum_i b_i Q_i) d\beta}, \quad i = X, Q, \quad (\text{B6})$$

with

$$b_X = \frac{2(x-1)x^2}{(x^2 - \bar{\rho}_X)^2} \left\{ -v_d^{-1} \ln \left[1 - v_d \left(1 - \frac{\bar{\rho}_X}{x^2} \right) \right] - 1 + \frac{\bar{\rho}_X}{x^2} \right\},$$

$$b_Q = \frac{(x-1)^2 x^2}{(x^2 - \bar{\rho}_Q)^2} \left\{ -v_d^{-1} \ln \left[1 - v_d \left(1 - \frac{\bar{\rho}_Q}{x^2} \right) \right] - 1 + \frac{\bar{\rho}_Q}{x^2} \right\}, \quad (\text{B7})$$

and the Q_i 's are defined in Eqs. (24) with the substitution $x = x_1 = x_2$. Furthermore, $\phi_j^k(\Omega, \Omega') \equiv \phi_j^k(\Omega', \Omega)$ in the uniaxial limit. For symmetry reasons $Q_Q = Q_X [x^2 - 2x(\sqrt{2} - 1)]/x^2$. The Gibbs function and chemical potentials in the nematic phase (N) become

$$\frac{G^N}{n_0 k_B T} = \frac{v_d^N}{x^2} \ln \frac{v_d^N}{x^2} + (1 - v_d^N) \ln(1 - v_d^N) - \frac{v_d^N}{x^2} \ln f_1$$

$$- \frac{2(x-1)}{x^2 - \bar{\rho}_X} \left[1 - v_d^N \left(1 - \frac{\bar{\rho}_X}{x^2} \right) \right] \ln \left[1 - v_d^N \left(1 - \frac{\bar{\rho}_X}{x^2} \right) \right]$$

$$- \frac{(x-1)^2}{x^2 - \bar{\rho}_Q} \left[1 - v_d^N \left(1 - \frac{\bar{\rho}_Q}{x^2} \right) \right] \ln \left[1 - v_d^N \left(1 - \frac{\bar{\rho}_Q}{x^2} \right) \right]$$

$$- 2 \frac{v_d^N}{x^2} [b_X(\bar{\rho}_X - x) + b_Q(\bar{\rho}_Q - \sqrt{2}x)], \quad (\text{B8})$$

$$\frac{\mu_s^N}{k_B T} = \ln(1 - v_d^N) - \frac{2(x-1)}{x^2 - \bar{\rho}_X} \ln \left[1 - v_d^N \left(1 - \frac{\bar{\rho}_X}{x^2} \right) \right]$$

$$- \frac{(x-1)^2}{x^2 - \bar{\rho}_Q} \ln \left[1 - v_d^N \left(1 - \frac{\bar{\rho}_Q}{x^2} \right) \right], \quad (\text{B9})$$

where we introduced subscript d in place of x to distinguish the solute particles. The basic quantities of the theory become

$$\bar{\rho}_{e1} = \bar{\rho}_{e2} = x^2 \mathcal{R} + x \equiv \bar{\rho}_X,$$

$$\bar{\rho}_q = [x^2 - 2x(\sqrt{2} - 1)] \mathcal{R} + \sqrt{2}x \equiv \bar{\rho}_Q, \quad (\text{B4})$$

where \mathcal{R} is given by

$$\frac{\mu_d^N}{k_B T} = \frac{2(x-1)}{x^2 - \bar{\rho}_X} \times \left\{ \left(\frac{2(\bar{\rho}_X - x)x^2}{(x^2 - \bar{\rho}_X)v_d^N - \bar{\rho}_X} \right) \ln \left[1 - v_d^N \left(1 - \frac{\bar{\rho}_X}{x^2} \right) \right] \right.$$

$$+ 2(\bar{\rho}_X - x) \left. \right\} + \frac{(x-1)^2}{x^2 - \bar{\rho}_Q} \times \left\{ \left(\frac{2(\bar{\rho}_Q - \sqrt{2}x)x^2}{(x^2 - \bar{\rho}_Q)v_d^N - \bar{\rho}_Q} \right) \right.$$

$$\times \ln \left[1 - v_d^N \left(1 - \frac{\bar{\rho}_Q}{x^2} \right) \right] + 2(\bar{\rho}_Q - \sqrt{2}x) \left. \right\}$$

$$+ \ln \frac{v_d^N}{x^2} - \ln f_1. \quad (\text{B10})$$

The isotropic phase chemical potentials are calculable in a straightforward way from Eqs. (34) and (35) by substituting $x = x_1 = x_2$:

$$\frac{\mu_s^I}{k_B T} = \ln(1 - v_d^I) - \frac{x^2 - 1}{x^2 - \bar{\rho}_d^I} \ln \left[1 - v_d^I \left(1 - \frac{\bar{\rho}_d^I}{x^2} \right) \right], \quad (\text{B11})$$

$$\frac{\mu_d^I}{k_B T} = \ln \frac{v_d^I}{x^2} - \frac{x^2 - 1}{x^2 - \bar{\rho}_d^I} \bar{\rho}_d^I \ln \left[1 - v_d^I \left(1 - \frac{\bar{\rho}_d^I}{x^2} \right) \right]. \quad (\text{B12})$$

APPENDIX C: SPECIAL CASE OF LONG RODS

The general theory developed in the present paper encompasses also another case of practical importance, i.e., a solution of long rods. This requires substitution of either $x_1 = 1$ or $x_2 = 1$. Let us briefly review the implications of the limit for the formalism. First we note that the molecular volume becomes x [instead of $(x_1 x_2)$ for plates], so the system volume is $n_0 = n_s + x n_r$ [cf. Eqs. (4)–(7)], where the subscript r is introduced to distinguish the rod limit. Equation (11) reduces to

$$\frac{v_{j+1}}{n_0} = \pi_d \pi_r^{x-1}, \quad (\text{C1})$$

as the process of inserting the test rod into a system is one dimensional and consists of putting in the anchor cell and the remaining $(x-1)$ cells (the edge cells).

Within the framework of the general theory, the $\{xyz\}$ frame is defined in such a way that the rod long axis points

along either (1) the x or (2) the y axis. In the former case the number of obstacles from the k th rod is solely given by \wp_{yz}^k :

$$\begin{aligned} \wp_{yx}^k &\equiv \wp_{e1}^k = x|\cos \alpha^k \sin \beta^k| + x|\cos \alpha^k \cos \beta^k \sin \gamma^k| \\ &\quad + |\sin \alpha^k \cos \gamma^k| + |\cos \alpha^k \cos \beta^k \cos \gamma^k - \sin \alpha^k \sin \gamma^k| \end{aligned} \quad (C2)$$

$$\simeq x(|\cos \alpha^k \sin \beta^k| + |\cos \alpha^k \cos \beta^k \sin \gamma^k + \sin \alpha^k \cos \gamma^k|) \quad (C3)$$

$$\simeq x(|\rho_{13}^{\Omega, \Omega'}| + |\rho_{12}^{\Omega, \Omega'}|) \equiv \wp_{yz}^k(\Omega, \Omega'); \quad (C4)$$

since $x \equiv x_1 \gg x_2 = 1$, the last term on the RHS of Eq. (C2) can be neglected. After some adjustment to recover proper behavior in the perfect order and disorder limits we have the projection of the k th rod [cf. Eq. (B2)]:

$$\wp_{yz}^k(\Omega, \Omega') \simeq (2x-1) \frac{|\rho_{13}^{\Omega, \Omega'}| + |\rho_{12}^{\Omega, \Omega'}|}{2} + 1, \quad (C5)$$

and with the use of Eq. (21) the system rod mean projection,

$$\begin{aligned} \bar{\wp}_{yz} &= (2x-1) \int \int w_{x1}(\Omega) w_{x1}(\Omega') \\ &\quad \times \frac{|\rho_{13}^{\Omega, \Omega'}| + |\rho_{12}^{\Omega, \Omega'}|}{2} d\Omega d\Omega' + 1. \end{aligned} \quad (C6)$$

Analogously, in the second case, $x \equiv x_2 \gg x_1 = 1$, the relevant quantity is the k th rod projection onto the xz plane:

$$\begin{aligned} \wp_{xz}^k &\equiv \wp_{e2}^k = x|\sin \alpha^k \sin \beta^k| + x|\sin \alpha^k \cos \beta^k \cos \gamma^k| \\ &\quad + \cos \alpha^k \sin \gamma^k| + |\cos \alpha^k \cos \beta^k \cos \gamma^k - \sin \alpha^k \cos \beta^k \sin \gamma^k| \end{aligned} \quad (C7)$$

$$\simeq x(|\sin \alpha^k \sin \beta^k| + |\sin \alpha^k \cos \beta^k \cos \gamma^k + \cos \alpha^k \sin \gamma^k|) \quad (C8)$$

$$\simeq x(|\rho_{23}^{\Omega, \Omega'}| + |\rho_{21}^{\Omega, \Omega'}|) \equiv \wp_{xz}^k(\Omega, \Omega'), \quad (C9)$$

which after an adjustment similar to the previous case becomes

$$\wp_{xz}^k(\Omega, \Omega') \simeq (2x-1) \frac{|\rho_{23}^{\Omega, \Omega'}| + |\rho_{21}^{\Omega, \Omega'}|}{2} + 1, \quad (C10)$$

giving the mean projection

$$\begin{aligned} \bar{\wp}_{xz} &= (2x-1) \int \int w_{1x}(\Omega) w_{1x}(\Omega') \\ &\quad \times \frac{|\rho_{23}^{\Omega, \Omega'}| + |\rho_{21}^{\Omega, \Omega'}|}{2} d\Omega d\Omega' + 1, \end{aligned} \quad (C11)$$

where the last term on the RHS of Eq. (C7) is set equal to a constant. The quantities $w_{x1}(\Omega)$ and $w_{1x}(\Omega)$ are the orientation distribution functions characteristic for each case. Note that the functional dependences on Ω of $w_{1x}(\Omega)$ and $w_{x1}(\Omega)$ are different from each other.

Refined molecular frame

Different functional forms of the rod equilibrium orientational distribution function and of the rod projection in cases (1) and (2) are a manifestation of the problem of choice of the appropriate molecular frame. In the case of rods these are the long axes which are orientationally ordered, and not the axes normal to the rod as assumed in the general case. Whatever the choice of the molecular frame, the mean equilibrium projection of the system rods onto the plane perpendicular to the long axis of the test rod, Eq. (C2) and Eq. (C7) must be quantitatively the same. In fact, it can be quite easily demonstrated that under properly chosen single Euler angle rotation the formalism developed for either case, i.e., the long axis parallel to x , or y , or z , can be transformed into the formalism developed for one of the other cases, and vice versa.

Let $\{xyz_i\}$ and $\{xyz_i^k\}$, $i=X, Y, Z$, denote, respectively, the test and the k th rod frames in the case when the rod is along the i axis of the molecular frame. For cases when the rod points along either (1) the x or (2) the y axis, the sets of Euler angles necessary to bring one frame into coincidence with another can be schematically represented, by analogy to Eq. (1), as

$$\begin{aligned} \{xyz_X\} &\xrightarrow{(\pi/2, 0, 0)} \{xyz_Y\}, \\ \{xyz_X^k\} &\xrightarrow{(\pi/2, 0, 0)} \{xyz_Y^k\}, \end{aligned} \quad (C12)$$

$$\{xyz_X\} \xrightarrow{\Omega^k} \{xyz_X^k\},$$

$$\{xyz_Y\} \xrightarrow{\Omega^{k'}} \{xyz_Y^k\}.$$

The required transformation of the rotation matrix is [cf. Eq. (A5)]

$$\begin{aligned} M_{ij}(\Omega^k) &= \sum_l \left(\sum_m M_{im}^{-1}(\pi/2, 0, 0) M_{ml}(\Omega^{k'}) \right) \\ &\quad \times M_{jl}^{-1}(\pi/2, 0, 0). \end{aligned} \quad (C13)$$

In this way not only does the full expression for \wp_{yz}^k [cf. Eq. (C2)] transform into \wp_{xz}^k in Eq. (C7), but also the relevant approximate forms, Eq. (C3) into Eq. (C8) and Eq. (C4) into Eq. (C9). Thus also the equilibrium $w_{1x}(\Omega)$ becomes $w_{x1}(\Omega)$ under transformation.

The same considerations affect transformations bringing the rod parallel to the z axis of the molecular frame, i.e., the convenient molecular frame for the rodlike solute. The relevant rotations are

$$\begin{aligned}
\{xyz_X\} &\xrightarrow{(0,-\pi/2,0)} \{xyz_Z\}, \\
\{xyz_X^k\} &\xrightarrow{(0,-\pi/2,0)} \{xyz_Z^k\}, \\
\{xyz_X\} &\xrightarrow{\Omega^k} \{xyz_X^k\}, \\
\{xyz_Z\} &\xrightarrow{\Omega^{k'}} \{xyz_Z^k\},
\end{aligned} \tag{C14}$$

and the transformation of the rotation matrix is

$$\begin{aligned}
M_{di}(\Omega^k) &= \sum_p \left(\sum_z M_{dz}^{-1}(0,-\pi/2,0) M_{zp}(\Omega^{k'}) \right) \\
&\times M_{ip}^{-1}(0,-\pi/2,0). \tag{C15}
\end{aligned}$$

Under the transformation, ϕ_{yz}^k for the rod in the direction of the x axis becomes ϕ_{xy}^k for the rod along the z axis, and the formalism becomes compatible with the theory for rods of Warner [8].

Using a molecular frame chosen such that the rod is along the z axis $\{xyz_Z^k\}$ we get [cf., e.g., Eqs. (C4) and (C5)]

$$\phi_{xy}^k \approx x(|\rho_{31}^{\Omega,\Omega'}| + |\rho_{32}^{\Omega,\Omega'}|) \approx (2x-1) \frac{|\rho_{31}^{\Omega,\Omega'}| + |\rho_{32}^{\Omega,\Omega'}|}{2} + 1. \tag{C16}$$

Minimization of the relevant Gibbs function with respect to the orientational order provides the equilibrium form for the distribution function:

$$\begin{aligned}
w_{1x}(\Omega) &\equiv w_z(\beta) = \frac{n\beta}{n_r} \\
&= \frac{\sin \beta \exp(-b_{xy} Q_{xy})}{\int d\beta \sin \beta \exp[-(b_{xy} Q_{xy})]} \\
&= \frac{\sin \beta \exp(-b_{xy} Q_{xy})}{f_1}, \tag{C17}
\end{aligned}$$

with

$$b_{xy} = \frac{(x-1)x}{(x-\bar{\phi}_{xy})^2} \left\{ -v_r^{-1} \ln \left[1 - v_r \left(1 - \frac{\bar{\phi}_{xy}}{x} \right) \right] - 1 + \frac{\bar{\phi}_{xy}}{x} \right\}, \tag{C18}$$

where

$$\begin{aligned}
\bar{\phi}_{xy} &= \int w_{1x}(\Omega') w_{1x}(\Omega) \phi_{xy}^k(\Omega, \Omega') d\Omega d\Omega' \\
&= (2x-1)\mathcal{R} + 1, \tag{C19}
\end{aligned}$$

with \mathcal{R} defined in Eq. (B5) and

$$Q_{xy} = 2(2x-1) \int w_z(\Omega') \frac{(|\rho_{31}^{\Omega,\Omega'}| + |\rho_{32}^{\Omega,\Omega'}|)}{2} d\Omega'. \tag{C20}$$

The chemical potentials in the nematic phase are

$$\frac{\mu_s^N}{k_B T} = \ln(1 - v_r^N) - \frac{(x-1)}{x - \bar{\phi}_{xy}} \ln \left[1 - v_r^N \left(1 - \frac{\bar{\phi}_{xy}}{x} \right) \right] \tag{C21}$$

and

$$\begin{aligned}
\frac{\mu_r^N}{k_B T} &= \ln \frac{v_r^N}{x} - \ln f_1 + \frac{x-1}{x - \bar{\phi}_{xy}} \times \left\{ \left(\frac{2x(\bar{\phi}_{xy} - 1)}{v_r^N(x - \bar{\phi}_{xy})} - \bar{\phi}_{xy} \right) \right. \\
&\times \ln \left[1 - v_r^N \left(1 - \frac{\bar{\phi}_{xy}}{x} \right) \right] + 2(\bar{\phi}_{xy} - 1) \left. \right\}. \tag{C22}
\end{aligned}$$

In the isotropic phase the mean projection becomes

$$\bar{\phi}_r^I = x + \frac{1}{2}, \tag{C23}$$

the $\frac{1}{2}$ term being due to the finite thickness of the rod. The relevant chemical potentials reduce to

$$\frac{\mu_s^I}{k_B T} = 2(x-1) \ln \left(1 + \frac{v_r^I}{2x} \right) + \ln(1 - v_r^I) \tag{C24}$$

and

$$\frac{\mu_r^I}{k_B T} = 2(x-1) \ln \left(1 + \frac{v_r^I}{2x} \right) \left(x + \frac{1}{2} \right) + \ln \frac{v_r^I}{x}. \tag{C25}$$

APPENDIX D: NUMERICAL PROCEDURE

Our numerical procedure was as follows. The efficiency of the algorithm in finding the equilibrium parameters depends strongly on the initial guess for the distribution function. Therefore, as the initial step, we searched for appropriate trial functions. It was a quite simple task, since the nematic phase is apolar, so that the distribution function has the property that $w(\beta) = w(\pi - \beta)$. Thus, averaging over the distribution, the integration can be limited to the range $\{0, \pi/2\}$ only, and the results then multiplied by 2. This substantially reduces the iteration procedure and provides the possibility of using any arbitrary function behaving reasonably in the range as the initial guess. Good examples of such useful trial distribution functions exploited in this work are $n_\beta/n_d = \cos^2 \beta$ (or $16.0 - 8.5\beta^2$) for disks, and $n_\beta/n_r = |\cos^3 \beta| + 0.85 \cos^4 \beta$ (or $16.83 - 10.0\beta^2$) for rods. In turn, for the theory of Warner [8] satisfactory results are obtained with $n_\beta/n_r = |\cos^3 \beta|$.

At the n th iteration step, for the instantaneous distribution function, the average projections [Eq. (B4) for disks or Eq. (C19) for rods] are calculated in the manner of Ref. [31]. Next, the exponents in Eq. (B7) [or Eq. (C18) for rods] are calculated. This completes the n th step. Results of the n th step are used next to calculate the $(n+1)$ th step instantaneous distribution function [Eq. (B6) with Eq. (24) for disks or Eq. (C17) with Eq. (C20) for rods; cf. Ref. [31]], and the whole iteration loop is repeated.

At the heart of each iteration step one performs the integration of \mathcal{R} with respect to $d\alpha$ and $d\beta'$ [cf. Eq. (B5)]. This integral is digitized with the aid of the trapezoidal quadrature formula. Integration intervals are divided into subintervals of lengths $\Delta\alpha = 2\pi/J_\alpha$ and $\Delta\beta = \Delta\beta' = \pi/2J_{\beta'}$, the latter for

(uniaxial) symmetry reasons, so that the integrated function is calculated at discrete points $\alpha_m = m\Delta\alpha$ ($m=0, \dots, J_\alpha$) and $\beta'_j = j\Delta\beta'$ ($j=0, \dots, J_{\beta'}$). Particular values of J_α and $J_{\beta'}$ are set to 1024 and 64, respectively; we found that two-fold increase of the J_α value does not change the final results to within the required accuracy of the calculations, and the value of $J_{\beta'} = 64$ is adopted after [31]. Since the distribution functions in Eqs. (B6) and (C17) are independent of α , it is sufficient to calculate the integral over α only once, and store the results in an auxiliary matrix, say, $W(i\Delta\beta, j\Delta\beta')$, where $i, j: j_{\beta'} \geq i, j \geq 1$ (cf. Ref. [31]).

After every iteration step convergence of the procedure is examined in the manner suggested in [31]. In the n th iteration step let the distribution function value for the i th grid point, β_i , be f_i^n . The n th step maximum single grid point relative deviation, which is a measure of the iteration convergence, or simply the “error,” is defined as

$$\epsilon_n = \frac{L}{1-L} \frac{\|f_i^n - f_i^{n-1}\|}{\|f_i^n\|} \quad (\text{D1})$$

where

$$L = \frac{\|f_i^n - f_i^{n-1}\|}{\|f_i^{n-1} - f_i^{n-2}\|} \quad (\text{D2})$$

and the normalization factor $\|f_i^n\|$ is defined as

$$\|f_i^n\| \equiv (\max\{f_i^n\}_{J_{\beta'} \geq i}). \quad (\text{D3})$$

It is assumed in our calculations that self-consistency is achieved once $\epsilon_n \leq 1 \times 10^{-5}$.

-
- [1] L. Onsager, Ann. (N.Y.) Acad. Sci. **51**, 627 (1949).
 [2] P. J. Flory, Proc. R. Soc. London, Ser. A **234**, 73 (1956).
 [3] W. Maier and A. Saupe, Z. Naturforsch. A **14**, 882 (1959).
 [4] M. Warner, J. Chem. Phys. **73**, 5874 (1980).
 [5] P. J. Flory, Adv. Polym. Sci. **59**, 1 (1984), and references therein.
 [6] J. K. Moscicki, Adv. Chem. Phys. **63**, 631 (1985).
 [7] M. Ballauff, Macromolecules **19**, 1366 (1986).
 [8] M. Warner, Mol. Cryst. Liq. Cryst. **80**, 79 (1982).
 [9] C. Counsel and M. Warner, Mol. Cryst. Liq. Cryst. **100**, 307 (1983).
 [10] M. Warner, Mol. Cryst. Liq. Cryst. **80**, 67 (1982).
 [11] P. J. Flory and G. Ronca, Mol. Cryst. Liq. Cryst. **54**, 289 (1979).
 [12] R. Alben, Mol. Cryst. Liq. Cryst. **13**, 193 (1971).
 [13] J. Herzfeld, J. Chem. Phys. **76**, 4185 (1982).
 [14] M. Wnek and J. K. Moscicki, Phys. Rev. E **53**, 1666 (1996).
 [15] M. Wnek and J. K. Moscicki, Phys. Rev. E **59**, 535 (1998).
 [16] D. Demus, in *Liquid Crystals*, edited by H. Stegemeyer, (Springer, New York, 1994), pp. 1–50.
 [17] W. Li and K. F. Freed, J. Chem. Phys. **101**, 519 (1994).
 [18] E. A. Di Marzio, A. J.-M. Yang, and S. C. Glotzer, J. Res. Natl. Inst. Stand. Technol. **100**, 173 (1995).
 [19] H. T. Davis, *Statistical Mechanics of Phases, Interfaces and Thin Films* (Wiley, New York, 1996), Chap. 6.
 [20] D. Sokolowska and J. K. Moscicki (unpublished).
 [21] M. E. Rose, *Elementary Theory of Angular Momentum* (Wiley, New York, 1957).
 [22] D. Sokolowska and J. K. Moscicki, Phys. Rev. E **54**, 5221 (1996).
 [23] D. Frenkel, Liq. Cryst. **5**, 929 (1989).
 [24] G. J. Vroege and H. N. W. Lekkerkerker, Rep. Prog. Phys. **55**, 1241 (1992).
 [25] D. Frenkel and B. M. Mulder, Mol. Phys. **55**, 1171 (1985).
 [26] Y. Rabin, W. E. McMullen, and W. M. Gelbart, Mol. Cryst. Liq. Cryst. **89**, 67 (1982).
 [27] M. A. Cotter, in *The Molecular Physics of Liquid Crystals*, edited by G. R. Luckhurst and G. W. Gray (Academic, New York, 1979), pp. 169–180.
 [28] J. G. J. Ypma and G. Vertogen, Phys. Rev. A **17**, 1490 (1978).
 [29] B. Tjpto-Margo and G. T. Evans, J. Chem. Phys. **94**, 4546 (1991).
 [30] D. Frenkel, B. M. Mulder, and J. P. McTague, Phys. Rev. Lett. **52**, 287 (1984).
 [31] J. Herzfeld, A. E. Berger, and J. W. Wingate, Macromolecules **17**, 1718 (1984).
 [32] P. J. Camp and M. P. Allen, J. Chem. Phys. **106**, 6681 (1997).
 [33] A. G. Vanakaras and D. J. Photinos, Mol. Cryst. Liq. Cryst. Sci. Technol., Sect. A **299**, 65 (1997).
 [34] A. G. Vanakaras, S. C. McGrother, G. Jackson, and D. J. Photinos, Mol. Cryst. Liq. Cryst. Sci. Technol., Sect. A **323**, 199 (1997).
 [35] A. G. Vanakaras, A. F. Terzis, and D. J. Photinos (unpublished).
 [36] Y. Galerne, A. M. Figueiredo Neto, and L. Liébert, Phys. Rev. A **31**, 4047 (1985).
 [37] N. Boden, J. Clements, K. A. Dawson, K. W. Jolley, and D. Parker, Phys. Rev. Lett. **66**, 2883 (1991).
 [38] H. W. Neuling, H. Stegemeyer, K. Praefcke, and B. Kohne, Z. Naturforsch., A: Phys. Sci. **42**, 631 (1987).
 [39] M. Cotrait, P. Marsau, C. Destrade, and J. Malthete, J. Phys. (France) Lett. **40**, L-519 (1979).
 [40] C. Destrade, N. H. Tinh, H. Gasparoux, J. Malthete, and A. M. Levelut, Mol. Cryst. Liq. Cryst. **71**, 111 (1981).
 [41] H. Zewdie, Phys. Rev. E **57**, 1793 (1998).
 [42] C. Carfagna, A. Roviello, and A. Sirigu, Mol. Cryst. Liq. Cryst. **122**, 151 (1985).
 [43] G. R. Luckhurst, R. A. Stephens, and R. W. Phippen, Liq. Cryst. **8**, 451 (1990).
 [44] R. Hashim, G. R. Luckhurst, F. Prata, and S. Romano, Liq. Cryst. **15**, 283 (1993).
 [45] A. P. J. Emerson, G. R. Luckhurst, and S. G. Whatling, Mol. Phys. **82**, 113 (1994).
 [46] W. L. McMillan, Phys. Rev. A **4**, 1238 (1971).
 [47] G. E. Feldkamp, M. A. Handschy, and N. A. Clark, Phys. Lett. **85A**, 359 (1981).
 [48] S. D. P. Flapper and G. Vertogen, Phys. Rev. A **24**, 2089 (1981).

- [49] M. C. Holmes, *Mol. Cryst. Liq. Cryst.* **124**, 131 (1985).
[50] N. Boden, R. J. Bushby, C. Hardy, and F. Sixl, *Chem. Phys. Lett.* **123**, 359 (1986), and references therein.
[51] H. N. W. Lekkerkerker, *Physica A* **176**, 1 (1991).
[52] E. Fontes, P. A. Heiney, M. Ohba, J. N. Haseltine, and A. B. Smith III, *Phys. Rev. A* **37**, 1329 (1988).
[53] I. Furó and B. Halle, *Phys. Rev. E* **51**, 466 (1995).
[54] J. Charvolin, *Nuovo Cimento D* **3**, 3 (1984).